Dear Editor,

We are pleased to submit our manuscript entitled "**High-thermally conductive AlN-based microwave attenuating composite ceramics with spherical graphite as attenuating agent**" for consideration in *Journal of Advanced Ceramics.* We confirm that this manuscript has not been published elsewhere and is not being considered for publication elsewhere. All authors have approved the manuscript and agree with submission to *Journal of Advanced Ceramics*. The authors have no conflicts of interest to declare.

This manuscript is mainly based on the exploitation of high-thermally conductive AlN-based microwave attenuation composite ceramics.

With the the fast growth of vacuum electronic devices towards high frequency, high power and high temperature, the development of high-thermally conductive microwave attenuation material is an inevitable trend in the future. Aluminum Nitride (AlN), by virtue of its integrated high thermal conductivity, high strength, high temperature stability and low dielectric constant, has drawn a great attention for preparing high-thermally conductive microwave attenuation ceramics by introducing kinds of attenuating agents such as metal conductors (W, Mo), semiconductors (SiC, TiO_2), or carbonaceous materials (graphite, carbon black, graphene and carbon nanotube). However, the highly sensitive thermal conductivity of AlN-based composite with the introduction of the second phase severely deteriorate the thermal conductive ability of the AlN-based attenuation ceramics. Despite the existing attenuating agents have been greatly proved to enhance the attenuation ability of the AlN-based composites,

no obvious breakthrough has been found in the preparing AlN-based attenuating ceramics with integrated strong attenuation and high thermal conductivity resulted from the introduction of a large number of heterogeneous interfaces.

In this regard, in view of the high electrical, thermal conductivity and great potential of graphite in the field of microwave absorption materials. Spherical graphite (SG) instead of traditional flake graphite was applied as attenuating agent to incorporate into AlN matrix. It is intended to use SG to improve the dielectric loss of AlN-based composites, simultaneously reducing the interface thermal resistance to ameliorate the thermal conductivity of AlN-based composites, then preparing a high-performance AlN-based microwave attenuation composite ceramic.

In this paper, high density (0-16 wt%) SG/AlN composites were prepared by hot-pressing sintering. The measurement and characterization of the as-sintered samples show that SG maintains its three-dimensional morphology within the sintered bodies, and SG introduction retards the sintering of the composites to some extent. The proper SG addition has a toughening effect on the composites with a maximum toughness of 3.8 $MPa \cdot m^{1/2}$ at 4 wt% sample. Attributing to its low-anisotropic thermal conductivity and small specific surface area, the minimum thermal conductivity of SG/AlN composites up to 76.82 $W \cdot m^{-1} \cdot k^{-1}$, showing the least impact on the thermal conductivity of AlN-based composites compared with existing reported attenuating agents. The dielectric constant and loss increased remarkably as SG content increases to 12 wt%, revealing an improved dielectric property with SG introduction. The reflection loss shows that the absorption ability of SG/AlN composites is strongly associated with SG

contents. The absorption ability can be enhanced with SG addition, while the high dielectric constant at higher SG content is unfavorable for impedance match and ultimately deteriorated the absorption ability. Overall, it is potential and feasible for employing SG as effective attenuating agent for preparing AlN-based composite attenuation ceramics with integrated strong attenuation, high thermal conductivity and low anisotropy. Undoubtedly, this article developed a novel attenuating agent for developing highly thermally conductive AlN-based microwave attenuation composite materials, simultaneously provided a valuable reference for the application of spherical graphite in the field of microwave absorption materials. Therefore, we believe that this article is very agreement with the innovative and advanced ceramics required by *Journal of Advanced Ceramics*, and which has never been reported before.

In order to improve the quality of this article, we suggested three suitable referees to review this paper, and listed as follows:

(1) **Jingxian Zhang**, jxzhang@mail.sic.ac.cn; Address: Shanghai Institute of Silicate, Chinese Academy of Sciences.

Suggested reason: Professor Zhang is an expert in the field of microwave attenuation materials, especially in the research of AlN-based microwave attenuation composite ceramics. So we believe he will be familiar with we have studied and give fair judgement to our manuscript.

(2) **Wenbo Bu**, wbbu@fudan.edu.cn, Address: Department of Materials Science, Fudan University.

Suggested reason: The literatures reported by Professor Bu in the early years were

highly associated with the preparation and performance of AlN-based microwave attenuating composite ceramics, we believe that he is proficient in the content that we have written.

(3) **Guobing Ying**, yinggb2010@126.com, Address: School of Mechanics and Materials, Hohai University.

Suggested reason: Professor Ying is an expert in the field of functional ceramics and serves as a referee for several journals that concerning ceramics research. We hope that he can provide valuable suggestions to improve the quality of our paper.

Finally, we deeply appreciate your consideration of our manuscript, and we look forward to receiving comments from the reviewers. If you have any queries, please don’t hesitate to contact me at the address below.

Thank you for your consideration.

Sincerely,

Xia Fang

Corresponding author:

Prof. Jian Yang

E-mail: yangjian1976@163.com

High-thermally conductive AlN-based microwave attenuating composite ceramics with spherical graphite as attenuating agent

Xia Fang[a, b], Lei Jiang[a, b], Limei Pan[a, b], Shuang Yin[a, b], Tai Qiu[a, b], Jian Yang[a, b, *]

a Jiangsu Collaborative Innovation Center for Advanced Inorganic Function Composites, China;

b College of Materials Science and Engineering, Nanjing Tech University, Nanjing 211816, China

*Corresponding author: E-mail: yangjian1976@163.com (Jian Yang)

Abstract: High-thermally conductive AlN-based microwave attenuating composite ceramics with spherical graphite (SG) as the attenuating agent were fabricated through hot-pressing sintering. The SG maintains its three-dimensional morphology within the sintered bodies, which considerably impedes the sintering of the composites to some extent but slightly influences on the growth of AlN grains. The addition of SG reduces the strength of the composites, but provides a moderate toughening effect at the optimal addition amount (3.8 $MPa \cdot m^{1/2}$ at 4 wt% SG). Benefiting from the low anisotropy, high thermal conductivity, and the three-dimensional morphology of SG, the composites exhibit a relatively higher thermal conductivity (76.82 $W \cdot m^{-1} \cdot k^{-1}$ at 10 wt% SG) compared with composites added with non-spherical attenuating agent. The dielectric constant and loss (8.2–12.4 GHz) increase remarkably as the amount of SG added increases up to 8 wt%, revealing that the incorporation of SG improves the dielectric property of the composite. The composite with 7 wt% SG exhibits the best absorption performance with a minimum reflection loss of -14 dB at 12.4 GHz and an effective

absorbing bandwidth of 0.87 GHz. The excellent overall properties of the SG/AlN microwave attenuating composites render them as a promising material for various applications. Moreover, SG has a great potential as an attenuating agent for microwave attenuating composites due to its strong attenuation upon integration, high thermal conductivity, and low anisotropy.

Keywords: Spherical graphite; Aluminum nitride; Thermal conductivity; Dielectric property; Microwave absorption

1 Introduction

A microwave attenuating material is a vacuum electronic material which is crucial in radars, early-warning aircrafts, and microwave measurement systems [1–6]. It absorbs electromagnetic waves within specific frequency bands and converts them into heat energy for the inhibition of sideband oscillation, broadening of bandwidth, and improving electromagnetic matching during operations. With the the fast development of vacuum electronic devices into high frequency, high power, and high temperature devices, it is indispensable for microwave attenuating materials to have a high thermal conductivity, in addition to an excellent microwave absorption capability, to enable them to conduct the heat energy efficiently and avoid damage to working devices caused by high temperature.

As a result of their outstanding characteristics such as high thermal conductivity, good mechanical properties, high temperature stability, and moderate dielectric constants, ceramic-based composite attenuating materials, such as BeO, MgO, Al_2O_3, and AlN matrix composite ceramics, have been one of the extensively for attenuation

materials [1]. Wherein AlN has been regarded as the most advantageous attenuating ceramic matrix by virtue of its high thermal conductivity (320 $W \cdot m^{-1} \cdot K^{-1}$), high strength, high insulation, non-toxicity and low out-gassing under a vacuum environment [1,2]. The preparation of AlN matrix microwave attenuating composite ceramics generally involves the introduction of metal conductors (W and Mo), semiconductors (SiC and TiO_2), or carbonaceous materials (graphite, carbon black, graphene and carbon nanotubes) to improve the dielectric loss of the AlN matrix composites, and enhance their microwave attenuation [3,4]. However, the thermal conductivity of AlN ceramics is highly sensitive to the introduction of a second phase, and all the pores, interfaces, grain boundary impurities, and crystal defects resulting from the addition of the attenuating agent greatly reduces the thermal conductivity of AlN-based composites [7–9].

To improve the thermal conductivity of AlN-based attenuating composites, highly thermally conductive metal attenuating agents have been employed. However, the inhomogeneous microstructure induced by the mismatching density between the AlN matrix and the metallic materials inevitably affects the thermal stability of the composite material. The wide band gap semiconductor SiC has been widely applied as an attenuating agent for preparing AlN-based attenuating composite ceramics. However, the addition of SiC not only increases the heterogeneous interface, but also generates a SiC/AlN solid solution. As a result, the SiC/AlN composites develop a large interface, high thermal resistance, and numerous crystal defects, which would cause severe phonon scattering and the deterioration of thermal conductivity of the SiC/AlN

composite attenuating ceramics [1,10,11].

In recent years, the lightweight carbonaceous nanomaterials with high electrical and thermal conductivity such as graphene and carbon nanotubes (CNTs), have been considered as promising attenuating agents for the preparation of attenuating composite materials based on a ceramic matrix [12–19]. Several studies have found that a small amount of incorporated graphene and CNTs greatly improves electrical conductivity and dielectric properties of AlN-based composite materials [7–9], making them potentially suitable attenuation agents for the preparation of AlN-based composite materials. Liang et al. [20] reported that, within the frequency range of 26.5–40.0 GHz, both the dielectric constant and dielectric loss of AlN/CNT composites increased significantly as the CNT content increased, and a high dielectric loss of 0.1−0.61 was achieved at 5 vol% CNT. Nonetheless, as CNTs have a very large specific surface area and a hollow tubular structure, they can adsorb a large amount of gas and may undergo out-gassing under a high vacuum environment, thus limiting their application in preparing vacuum electronic materials [21,22]. Graphene has an ultra-high thermal conductivity along the in-plane direction, while its layered structure readily produces a large heterogeneous interface between AlN matrix and graphene, which greatly reduces the thermal conductivity of AlN/graphene composite materials [7, 8]. Yin et al [23] reported that the thermal conductivity of graphene platelets/AlN composites sharply decreased from 58.21 to 13.84 $W \cdot m^{-1} \cdot K^{-1}$ as the graphene content increased from 0 to 9.5 wt%. One/two-dimensional (1/2D) carbonaceous nanomaterials are generally anisotropic [7,24], which is detrimental to the uniform heat dissipation of the material. Although

various potential attenuating agents, such as metal conductors, semiconductors, and carbonaceous materials, have been studied, none of them are without anisotropy and are therefore not suitable for the preparation of a highly thermally conductive AlN-based attenuating composite materials with no anisotropy. To improve the work reliability of microwave attenuating materials in future work, it is important to exploit an attenuating agent that can satisfy the demand of both high thermal conductivity and strong attenuation of attenuating materials.

Among the previously reported attenuating agents, graphite is a traditional carbonaceous material with an excellent electrical conductivity (~ 10^6 s/m), thermal conductivity (~ 2200 $W \cdot m^{-1} \cdot K^{-1}$) [25], high thermal stability and low cost, hence, it is considered as a promising material for the preparation of materials with strong attenuation [26–34]. Historical studies have shown that the introduction of a small amount of graphite can improves the dielectric property and microwave absorption performance of the composites incorporated with graphite [29–34]. Torgut et al. [32] found that the incorporation of graphite into a polymer matrix significantly enhanced the polarization loss of the composites, and the ε' value of the 10wt% composite was 80.5 higher than that of the monolithic polymer material. Sun et al. [33] fabricated SiC/graphite composites based on a porous SiC matrix, and they found that introducing graphite from 1 wt% to 7 wt% increased the electrical conductivity of the composite by five orders of magnitude. Moreover, the incorporation of graphite resulted in the multiple reflection of the electromagnetic waves inside the material, improving the electromagnetic shielding performance of the SiC/graphite composite. Zhang et al. [34]

observed that when the graphite/geopolymer ratio was 12, the minimum reflection loss (RL_{min}) of the graphite/geopolymer composite reached -65 dB at a frequency range of 2–18 GHz and at a thickness of 4.15 mm thickness. However, the application of graphite in preparing AlN matrix composite attenuating materials has not been reported in detail until now. Moreover, in all of the reports on composite absorption materials filled with graphite, the flake graphite is the dominantly employed. Coinciding with its 2D structure of two-dimensional materials, the high aspect ratio of flake graphite can also result in numerous heterogeneous interfaces inside the matrix, just like graphene, thereby limiting the improvement of the thermal conductivity of the composite. Moreover, the composites filled with 2D flake graphite also suffer from the anisotropic thermal, electricity, and dielectric properties [25, 35–38]. For example, Li et al. [38] employed the squeeze casting method to fabricate graphite flakes/Al composites and found that as the graphite content varied from 40 to 70 vol%, the thermal conductivity of the composites increased from 544 to 714 $W \cdot m^{-1} \cdot K^{-1}$ in the direction parallel to the plane of the graphite layers but decreased from 104 to 31 $W \cdot m^{-1} \cdot K^{-1}$ in the direction perpendicular to the plane of the graphite layers, resulting from the high interfacial thermal resistance, low thermal conductivity (6 $W \cdot m^{-1} \cdot K^{-1}$) and the anisotropy caused by the addition of flake graphite. This suggests that there is a great limitation on the preparation of high-performance composite attenuating ceramics with high thermal conductivity and low anisotropy when flake graphite is employed as the attenuating agent. And to the best of our knowledge, which remains a great challenge to date.

In this work, considering the high electrical and thermal conductivity and the

microwave absorption property of graphite, spherical graphite, instead of the traditional flake graphite, was chosen as the attenuating agent in the preparation of AlN-based attenuating composite ceramics with strong attenuation, high thermal conductivity, and low anisotropy. SG is a granulated from of graphite, which not only enjoys excellent thermal and electrical properties similar to flake graphite, but also has a low anisotropy as opposed to flake graphite. More importantly, the spherical morphology of SG results in its relatively small aspect ratio, which can potentially reduce the heterogeneous interfaces between the graphite particles and the AlN matrix and their adverse effect of interfacial thermal resistance on the thermal conductivity of the AlN-based composite. Owing to its high electrical conductivity, low specific surface area, chemical resistance, high crystallinity and high theoretical lithium insertion capacity, SG is widely utilized to as a substitute for the traditional flake graphite for the preparation of the battery negative electrodes in batteries [39,40]. Regrettably, as far as we know, there are few reports on the preparation of ceramic matrix composite materials filled with spherical graphite.

To explore the potential and feasibility of employing SG as highly effective attenuating agent for the preparation of AlN-based composite attenuating materials, the effects of the mass fraction of SG on the sintering, mechanical, thermal, dielectric, and absorption properties of the SG/AlN composites were systematically studied. The obtained SG/AlN composites exhibited a low anisotropy, excellent thermal conductivity, and strong dielectric loss and absorption ability, which demonstrate their potential as high-performance attenuation materials for future application after further optimization.

2 Experimental Process

2.1 Preparation of SG/AlN composite ceramics

Commercial AlN (1−2 μm, Liaoning Desheng Special Ceramics Manufacturing Co., Ltd), Y_2O_3 (d_{50} = 7 μm, purity 99.95 %, Shanghai Yuelong Chemical Factory), and SG (d_{50} = 6 μm, Qingdao Haida Graphite Co., Ltd.) were used as the raw materials. The microscopic morphology of the spherical graphite is depicted in Figure 1. The SG particles are oval, and they have a significant difference from the layer structure of flake graphite.

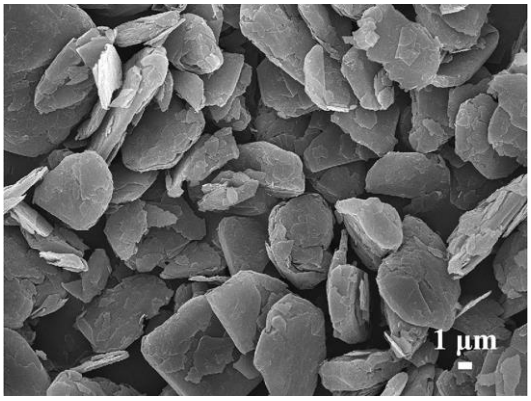

Fig. 1 Micro-morphology of spherical graphite raw material

The amount of the sintering aid Y_2O_3 was fixed at 4 wt%, and the SG content was varied from 0 to 16 wt%. The preparation process of the SG/AlN composites is schematically shown in Figure 2. First, the AlN and Y_2O_3 powders was ball-milled for 4 h in a planetary ball mill at a rotating speed of 160 rpm. Thereafter, they were dried at 80 ℃ for 24 h, ground, and then sieved through a size 60 mesh. Varying amounts of SG powder was mixed with the AlN-Y_2O_3 composite powder in anhydrous ethanol, and the mixture was combined under magnetic stirring (S10-3, Shanghai Sile Equipment Co., Ltd., China) and mechanical stirring (JJ-1, Jiangyin Poly Research Equipment Co., Ltd.,

China) for 2.5 h at 750 rpm. The mixture was dried at 120 ℃ for 8 h, and the resultant powders were sieved through a size 60 mesh. The as-prepared composite powders with different SG contents were loaded into graphite molds and then hot-pressing sintered under a nitrogen (N_2) atmosphere, with a sintering temperature of 1900 ℃, uniaxial pressure of 25 MPa, and holding time of 1 h. Finally, the as-sintered samples were cooled to room temperature and then taken out of their molds.

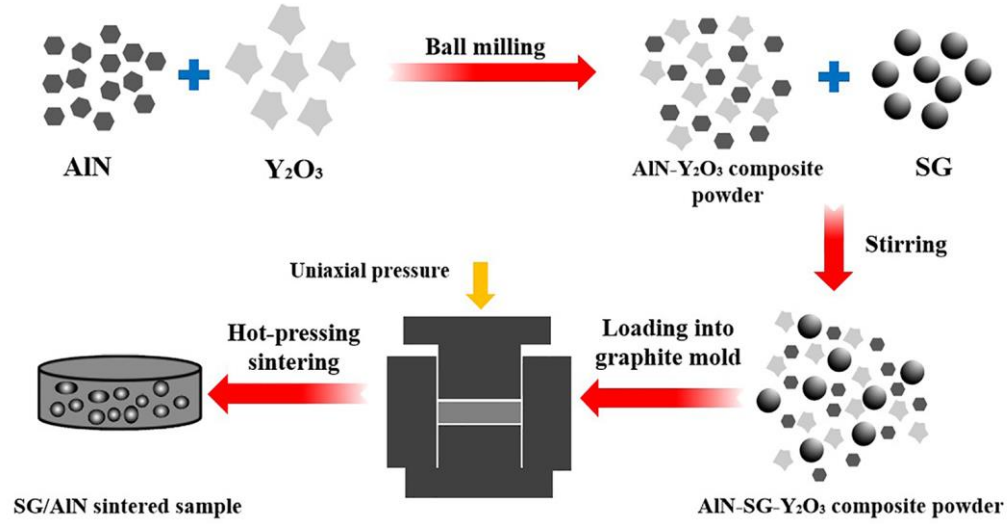

Fig. 2 Schematic of the preparation process for fabricating the SG/AlN composites

2.2 Testing and Characterization

The phase composition of the as-prepared SG/AlN composites was detected using X-ray diffraction (XRD, Smartlab, Japan) analysis. The X-ray photoelectron spectroscopy (XPS, AXIS Ultra DLD, Kratos, UK) was carried out to determine the chemical composition of the surface of the sample. The bulk density of the sintered sample was measured by Archimedes method, and then the bulk density of the sample was divided by the corresponding theoretical density to obtain the relative density, wherein the theoretical density of the composites was calculated in accordance with the rule of mixtures, assuming the densities of 3.26 $g \cdot cm^{-3}$ for AlN, 5.01 $g \cdot cm^{-3}$ for Y_2O_3,

and 2.25 g·cm^{-3} for SG. The flexural strength of the sample with a dimension of 4 × 3 × 36 mm^3 was tested using the three-point bending method at a loading rate of 0.5 mm·min^{-1}. To test the fracture toughness of the sample, the single edge notch beam method was carried out at a loading rate of 0.05 mm·min^{-1} for a sample with dimensions of 4 × 2 × 30 mm^3, with a groove depth of 2 mm and width of 0.1 mm. A field emission scanning electron microscope (FESEM, SU8010, Hitachi, Japan) equipped with an energy dispersive system (EDS) was used to analyze the fracture morphology and chemical composition of the sample. The thermal diffusion coefficient α of the sample (Φ 12.7 mm × 2 mm) was determined using a laser thermal conductivity meter (LFA447, Netzsch, Geramany) under the protection of helium atmosphere, and the thermal conductivity λ of the sample was calculated by Equation (1) [41]:

$$\lambda = \alpha \times C_p \times \rho \quad (1)$$

where ρ is the bulk density of the sample, and C_p is the heat capacity. Each sample subjected to thermal analysis was tested for three times, and the mean value was calculated. To investigate the dielectric properties and microwave absorption properties of the samples, the waveguide method with a vector network analyzer was used to test the electromagnetic parameters of the sample (22.86 × 10.16 × 2.5 mm^3) in the X-band (8.2–12.4 GHz).

3 Results and Discussion

3.1 Phase Composition

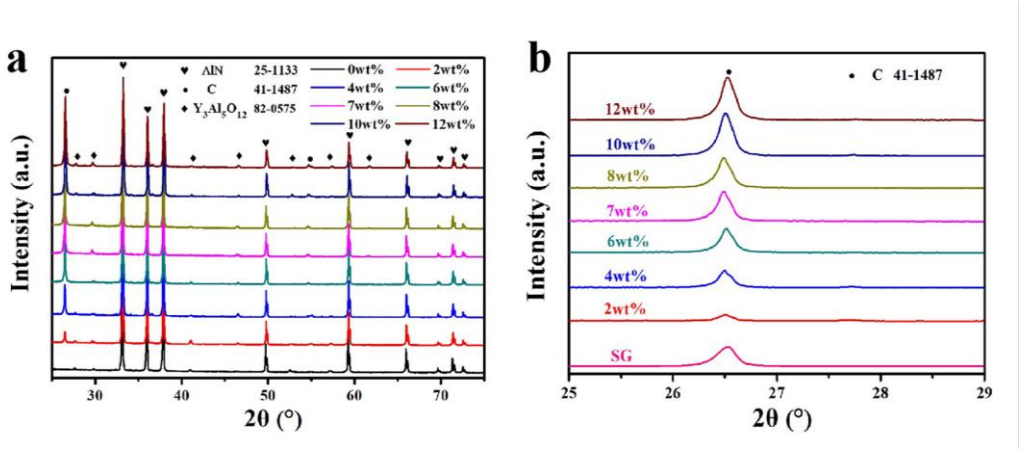

Fig. 3 (a) XRD patterns of SG/AlN composites with different SG contents, (b) XRD patterns of SG raw powder and SG/AlN composites with different SG contents at 25 to 29 degrees

The XRD patterns of the as-sintered SG/AlN composites with various SG contents are presented in Figure 3(a). The main phases in the monolithic AlN ceramic are AlN and $Al_5Y_3O_{12}$, while the main phases in the SG/AlN composites are AlN, carbon (C), and $Al_5Y_3O_{12}$. No other carbon-containing compound was detected, illustrating that SG did not react with any other phases during the sintering process. The XRD patterns of the SG raw material and SG/AlN composites with various SG contents within a small 2θ angle range are shown in Figure 3(b). Visibly, the diffraction peak of C becomes stronger as the SG content increases, and the position of the C diffraction peak in the composite material did not show a significant change with that in the SG raw material. This indicates that SG maintains as its original graphitic structure in the sintered sample. The existence of $Y_3Al_5O_{12}$ is ascribed to be the reaction between Y_2O_3 and Al_2O_3 that exists on the surface of AlN, which not only promotes the liquid phase sintering of the AlN-based composite under a relatively low temperature, but also effectively removes the oxygen impurities in the lattice of AlN, thereby enhancing the thermal conductivity of the AlN-based composite ceramics [42,43].

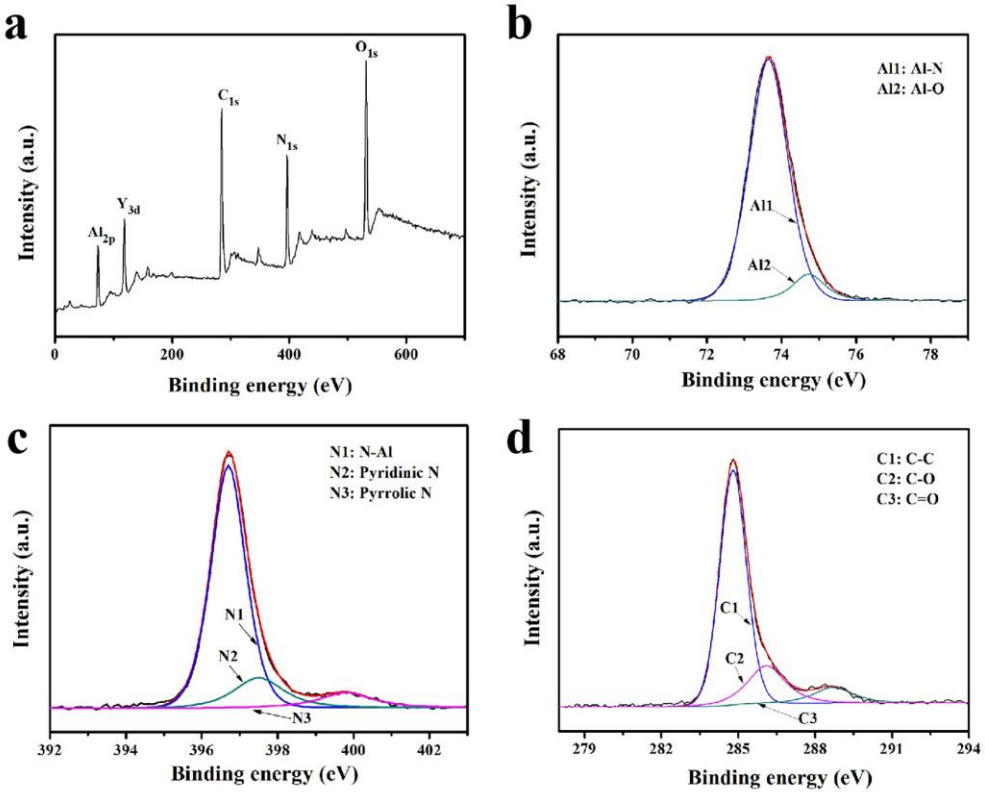

.Fig. 4 (a) XPS survey spectra of 4 wt% composite, (b–d) are the spectra of Al 2p, N 1s and C 1s, respectively

To further identify the chemical forms and interactions of each elements in the SG/AlN composite, the XPS survey spectra of the 4 wt% composite were obtained and presented in Figure 4. Several typical peaks for Al 2p, C 1s, N 1s, Y 3d, and O 1s can be clearly identified in Figure 4(a). In the XPS spectrum of Al 2p, as shown in Figure 4(b), the intensity of peaks at 73.65 eV and 74.73 eV correspond to the Al-N and Al-O bonds, respectively [44]. It can be inferred that the $Y_3Al_5O_{12}$ is responsible for the formation of Al-O. The N element mainly exists in the form of the N-Al bond (396.7 eV) in the sintered body [44]. In addition, the two slight and minor peaks appear at 397.5 eV and 399.8 eV correspond to pyridinic N [45,46] and pyrrolic N [47], respectively. This may be attributed to that a few C atoms which were doped into the AlN lattice and replaced the N atoms [48]. The C 1s spectrum can be divided into C-C (284.8 eV) [45,49], C-O

(286.1 eV) and C=O (288.7 eV) bonds [50]. The presence of carbon-oxygen bonds may be due to a small amount of oxidation of graphite during the drying process. Nevertheless, no other C bonds were found in the composite, further confirming that SG still maintains its original graphitic structure within the sintered body, and no N doping of the SG occurred even after sintering under a N_2 protective atmosphere.

3.2 Sintering Properties and Microstructure

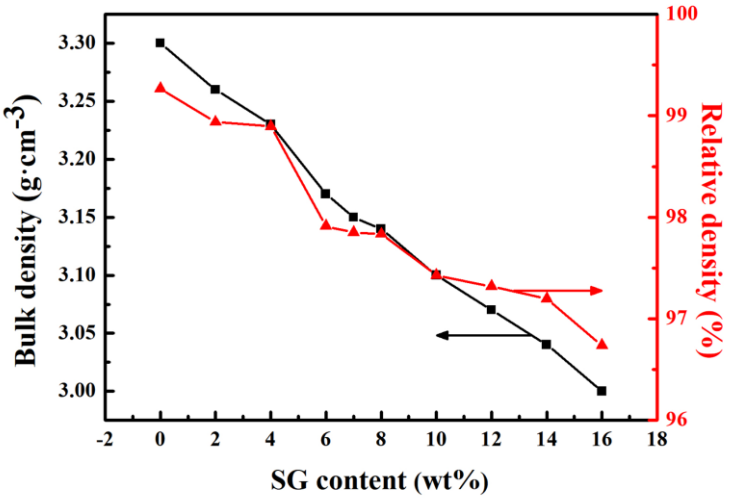

Fig. 5 Bulk density and relative density of SG/AlN composites with different SG contents

The bulk density and relative density of the SG/AlN composites with varying SG contents are shown in Figure 5. As the SG content increases from 0 wt% to 16 wt%, the bulk density and relative density of the composites decrease monotonously from 3.30 $g \cdot cm^{-3}$ to 3.00 $g \cdot cm^{-3}$ and 99.50 % to 96.73 %, respectively. The descend of relative density indicates that the SG addition significantly inhibits the sintering process of the SG/AlN composites. To explain the decrease in density of the composite as the amount of SG increases, the micro-morphology, location, and distribution of SG particles within the materials, the microstructure and chemical composition of the SG/AlN composites

were further characterized through SEM, EDS, and element mapping [48,51,52].

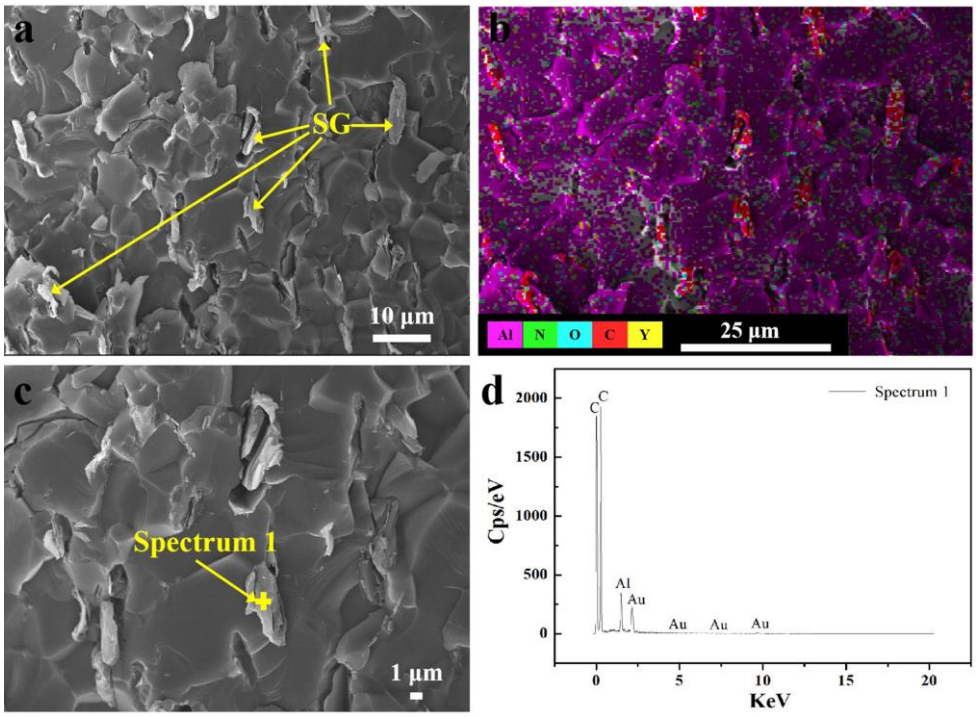

Fig. 6 (a) Microstructure, (b) EDS mapping, (c) high-resolution microstructure and (d) EDS diagrams of 4 wt% SG/AlN composite without ultrasonic cleaning

The SEM, EDS, and element mapping diagrams of the composite with 4 wt% SG are provided in Figure 6. The red area in Figure 6(b) indicates the SG particles, as confirmed by the combined analysis of element mapping and EDS. The SG particles, with a significantly different morphology from the AlN matrix, can be well distinguished in Figures 6(a) and (c). Figure 7 shows the fracture morphology of composites containing 4, 6, 10, 12 wt% SG, in which the yellow arrow indicates the SG particles. Compared with that of the pristine SG shown in Figure 1, the micro-morphology of the SG inside the sintered sample suffered some damage and exhibited a pronounced deformation, which can be attributed to the uniaxial pressure applied during the sintering process. Moreover, a significant agglomeration of SG

particles can be observed in the composites with 10 wt% and 12 wt% SG, implying that at high SG contents, the SG particles experience an increased difficulty in dispersion. Nonetheless, most of the SG particles inside the composites maintain their three-dimensional morphology after sintering, which is an obvious distinction from the 2D morphology of flake graphite [25, 27, 33].

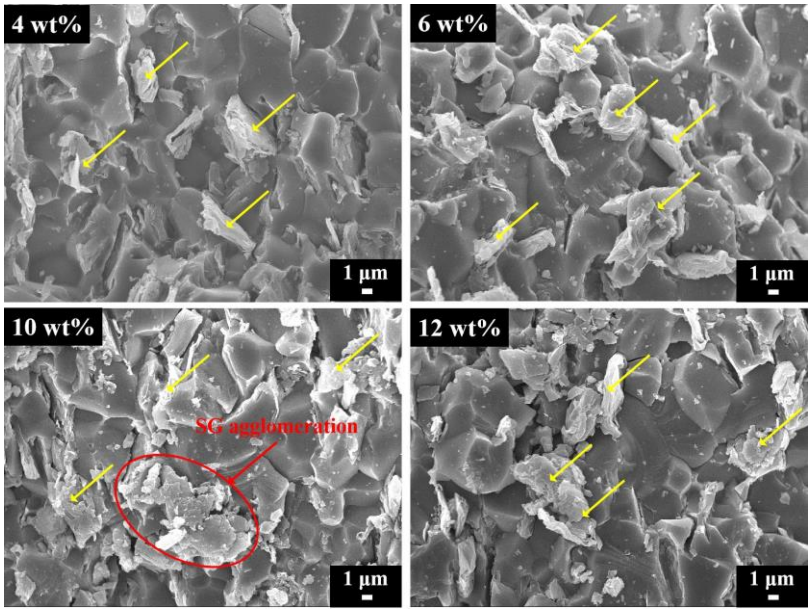

Fig. 7 Microstructure diagrams of SG/AlN composites with 4, 6, 10, 12 wt% SG, the yellow arrow indicates SG particle

To more clearly observe the location and distribution of SG inside the AlN matrix, the fracture surfaces of the sintered samples with 0 wt% to 12 wt% SG, were ultrasonically cleaned and then characterized using SEM and EDS analysis. As is shown in Figure 8, the SG showed a clear fault-like structure after ultrasonication. Meanwhile, the fine AlN particles and SG particles on the fracture surface of the ultrasonicated sample were cleared away, showing a clearer fracture morphology in comparison with the non-ultrasonicated sample. Figure 9 shows the fracture morphology of the composites containing different SG contents. Overall, the SG particles and AlN grains,

although tightly bonded, showed significantly different morphologies, which can be clearly distinguished in all the composites. The SG particles were distributed homogeneously in the AlN matrix. The Figure 9 further confirms that the micro-morphology of SG was slightly deformed after sintering. Nevertheless, none of these composites exhibited a pronounced behavior based on orientation, whether parallel or perpendicular to the pressure directions inside the sintered body. This is obviously differed from the orientated flake graphite in the AlN/graphite composite reported by Zhang et al [25], suggesting that orientation alignment and anisotropy can be alleviated to some extent by using spherical graphite.

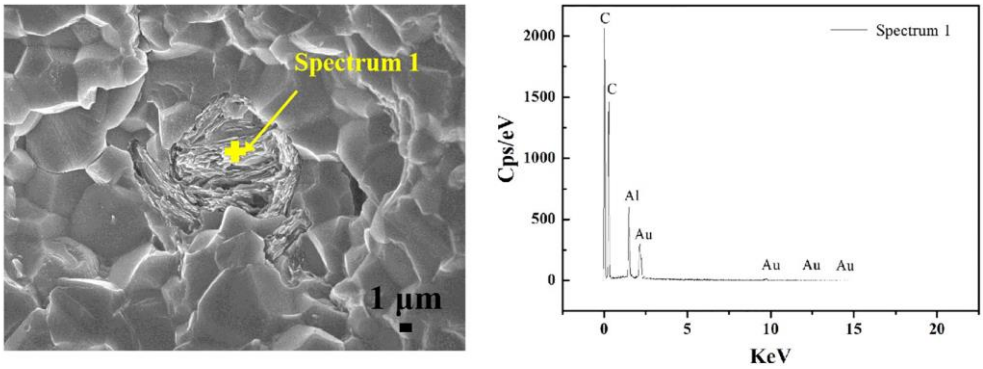

Fig. 8 Microstructure (ultrasonic cleaning) and EDS diagrams of 4 wt% SG/AlN composite

As shown in Figure 9, the average AlN grain size of a monolithic AlN ceramic is 6 μm, while that of the composite with 12 wt% SG is 5 μm. Compared to the decrease in the AlN grain size from 6.5 μm to 3.5 μm, as the graphene content increased from 0 to 7.28 vol% (5 wt%), in graphene/AlN composites prepared via hot-pressing sintering [8], the introduction of SG into the AlN matrix only slightly inhibited the growth of AlN grains, which may be ascribed to the lower SG/AlN grain boundary interface in SG/AlN composites relative to that of the AlN-based composites containing 2D flake materials.

The fewer SG/AlN interfaces sufficiently decrease the adverse impact of the incorporation of SG on the AlN mass transfer, thereby alleviating the inhibition of AlN grain growth. As the amount of SG incorporated increases, the SG/AlN heterogeneous interface grows and has a non-negligible effect on the mass transfer process of AlN and the migration process in the AlN grain boundary. These hinder the sintering process of the materials, increasing the number of pores within the material and accordingly decreasing the densification.

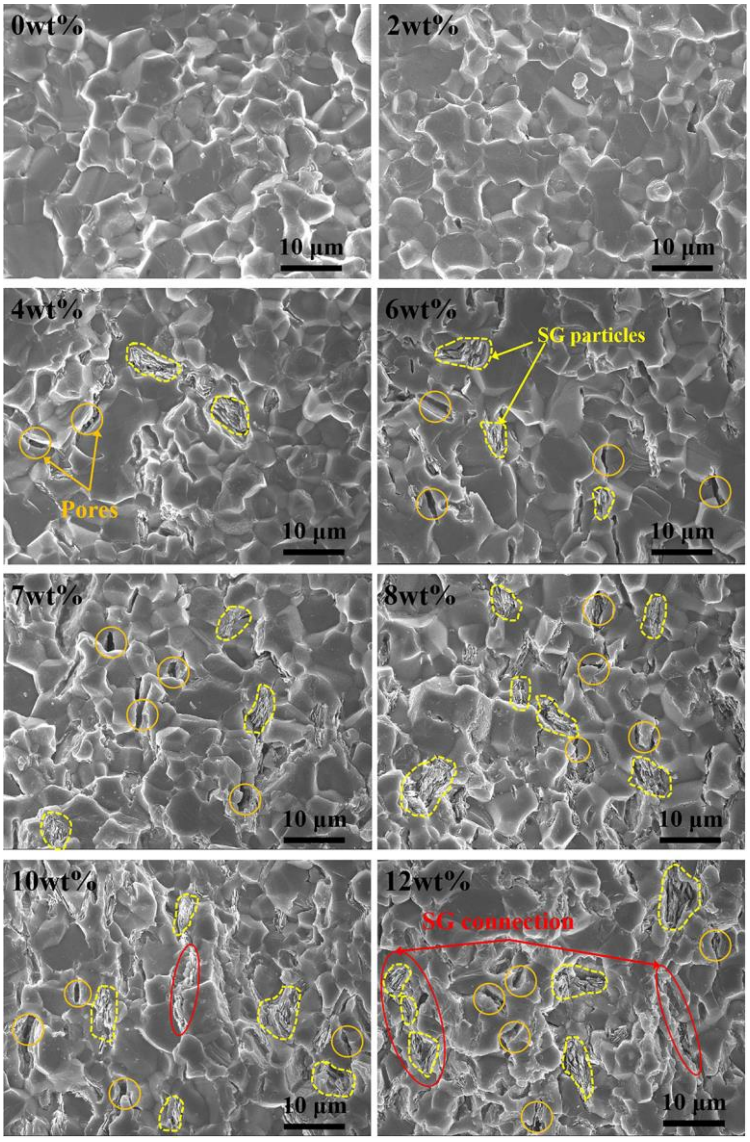

Fig. 9 Fracture morphology of SG/AlN composites with different SG contents

3.3 Mechanical Properties

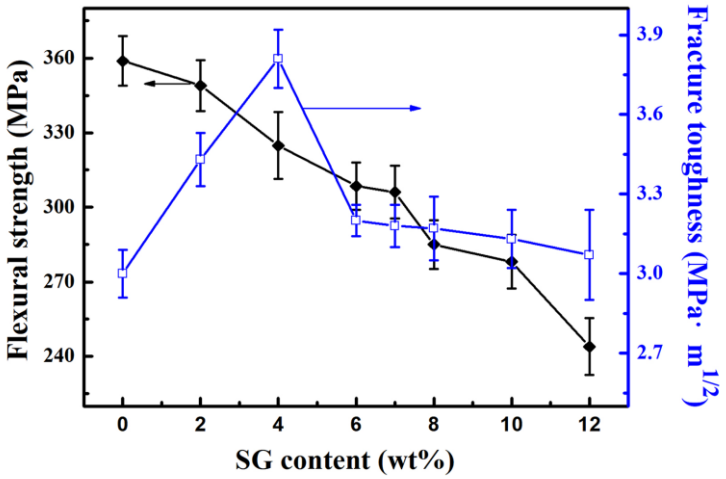

Fig. 10 Mechanical properties of SG/AlN composites with different SG contents

To evaluate the mechanical properties of the SG/AlN composite ceramics, the flexural strength and fracture toughness of the SG/AlN composite as a function of SG content were obtained and shown in Figure 10. The strength of the composites decreases monotonically from 358 MPa to 240 MPa as the amount of SG increases from 0 wt% to 12 wt%, indicating that the addition of SG causes damage to the flexural strength of the composite. According to the fracture morphology analysis, the decrease in the strength is mainly caused by the increasing number of pores in the composite and the weakening of the interfacial bonding between the SG particles and AlN matrix as more SG is incorporated into the composite, which greatly reduce the energy required for crack propagation during the fracture process.

The fracture toughness of the composite material exhibits an increasing trend at first and then decreases as the SG increases, reaching the maximum of 3.8 MPa·$m^{1/2}$ at 4 wt% SG, which is 27 % more than that of the monolithic AlN ceramic, revealing that a

moderate addition of SG has a certain toughening effect on the SG/AlN composites. Fracture toughness is the ability of a material to resist crack propagation, and the main toughening mechanism that occurs in the SG/AlN composites can be determined through the SEM images of the fracture morphology. As shown in Figure 9, SG particles are dispersed homogeneously inside the composites, and composites with low SG content exhibit a high densification, which endows a strong interfacial bonding force between the SG particles and the AlN matrix. The high-resolution fracture morphology of the sample with 4 wt% SG after ultrasonic cleaning and without ultrasonic cleaning are presented in Figures 11(a) and (b), respectively. As visible in Figure 11(a), the SG particles are tightly pinned inside the AlN grains, which induce a pinning effect in the material and consequently promote crack deflection during the crack propagation stage. In addition, the Figure 11(b) reveals that there are numerous extracted SG particles on the fracture surface, which is mainly because the SG particles were slightly deformed during the sintering process and became non-equiaxed particles. Considering the behavior of composite ceramics toughened by non-equiaxed materials such as graphene, carbon fibers, and CNTs [8], the extracted SG implies that numerous SG bridging and pulling-out have been generated during the fracture process, thus consuming a large quantity of fracture energy. This phenomenon reasonably toughens the SG/AlN composites. However, at higher SG contents, the increase in the number of pores and the consequent decrease in density weaken the interfacial bonding between the AlN grains and SG particles, which has a significant and detrimental effect on the mechanical properties of the composite. As a result, a decreased fracture toughness is

observed when the SG content exceeds 4 wt%.

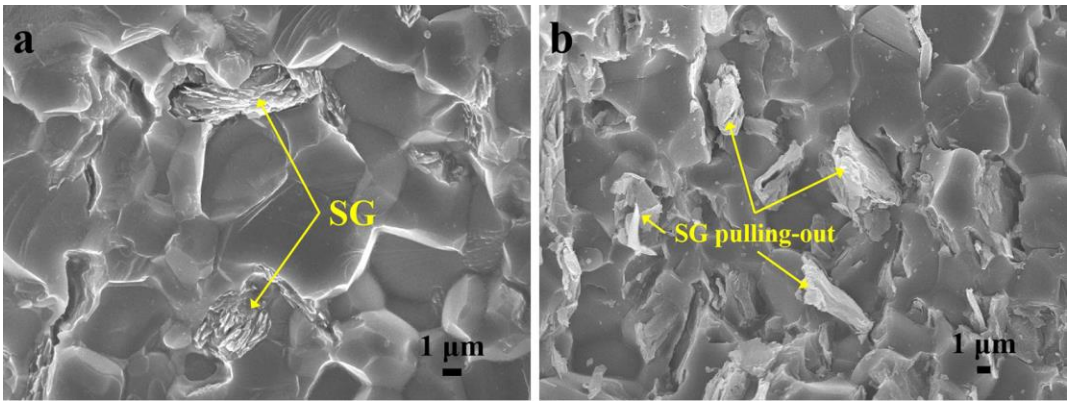

Fig. 11 High-resolution fracture morphology of 4 wt% SG/AlN composite, (a) ultrasonic cleaning, (b) without ultrasonic cleaning

3.4 Thermal Properties

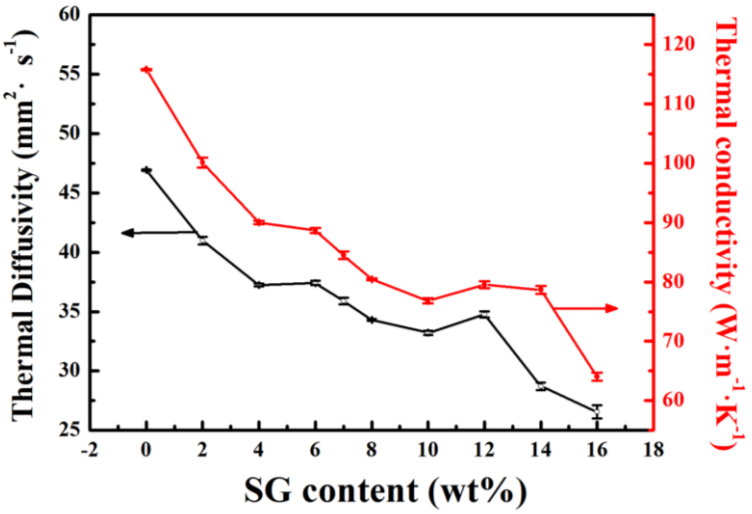

Fig. 12 Thermal diffusivity and thermal conductivity of SG/AlN composites with different SG contents

To investigate the thermal properties of the SG/AlN-base composites, the α and λ of the SG/AlN composite ceramics with varying SG contents were measured and are presented in Figure 12. Generally, both the α and λ values of the composite ceramics exhibit a remarkable downtrend as the SG content increases from 0 to 16 wt%. The α

and λ of monolithic AlN ceramic are 46.93 $mm^2 \cdot s^{-1}$ and 115 $W \cdot m^{-1} \cdot k^{-1}$, respectively. The α of the composite with an SG content of 6, 8, and 10 wt% is 37.41, 34.30, and 33.22 $mm^2 \cdot s^{-1}$, respectively, while the λ of the composite with an SG content of 6, 8, and 10 wt% is 88.65, 80.44, and 76.82 $W \cdot m^{-1} \cdot k^{-1}$, respectively. When the SG content of the composite increases to 6 wt%, the α and λ decrease, and when the SG content further increases to 8 wt%, they drop sharply. As the SG content further increases to 10 wt%, the α and λ slightly decline, revealing that the addition of SG is detrimental to the thermal properties of the SG/AlN composites. Surprisingly, the α and λ of the composite with 12 wt% SG exhibit an increase to 34.76 $mm^2 \cdot s^{-1}$ and 79.53 $W \cdot m^{-1} \cdot k^{-1}$, respectively, instead of decrements. Further addition of SG to 16 wt% leads to the minimum α and λ values of 26.54 $mm^2 \cdot s^{-1}$ and 64.04 $W \cdot m^{-1} \cdot k^{-1}$, respectively.

As a covalently bonded inorganic compound, the λ of AlN crystals is strongly associated with phonon heat conduction [53], as described by the following Equation [54]:

$$\lambda = 1/3cvl \quad (2)$$

where c is specific heat capacity, v is the mean velocity of the phonon, and l refers to the mean free path of the phonon. Enhanced phonon scattering results in the decrease of l, thereby reducing λ [53]. The phonon scattering in AlN-based composites mainly originates from various defect-phonon scattering, such as vacancies, dislocations, grain boundary interfaces, and pores [7]. For the SG/AlN composites, the growing SG/AlN interface as SG loading increases enhances the scattering of phonons and generates more interfacial thermal resistance, thus inducing a negative effect on the λ of the

composite [8,54,55]. In addition, as the sources of scattering, the increased in the number pores at higher SG contents also contributes to the decrease in λ. The effect of porosity on λ of a material can be expressed as follows [56]:

$$\lambda=\lambda_0(1-3/2\Phi) \quad (3)$$

where λ_0 represents the thermal conductivity of a dense material, and Φ is the porosity. Equation (3) shows that λ has an inverse relationship with the Φ of a material, hence, the increasing number of pores as the SG loading increases also contribute a lot to the degradation of the λ of the SG/AlN composites. The abnormal increase in λ at 12 wt% SG may be ascribed to the formation of partial thermal-conduction paths caused by the connection of SG particles at higher SG contents. However, the further addition of SG seriously decreases the densification and increases the number of pores in the composites, thus resulting in a dramatically decrease in the λ value to 64.04 $W\cdot m^{-1}\cdot k^{-1}$ at 16 wt% SG.

In comparison with other AlN-based attenuating ceramics, the thermal properties of AlN-based composites containing different attenuating agents are tabulated in Table 1. Generally, the λ of the SG/AlN composites are significantly higher than that of AlN/SiC attenuating composite ceramics (40 to 70 $W\cdot m^{-1}\cdot k^{-1}$, [1,10,11]) at the same content of the second phase. Simultaneously, in comparison to the AlN-based composites containing 1/2D carbon materials, such as graphene and carbon nanotubes, as the second phase [7–9], at the same content, the SG/AlN composite shows a relatively higher λ as well. For example, the λ of the AlN/graphene composite containing 0.1 vol% (0.07 wt%) graphene prepared by Simsek et al. [7] is only 74 $W\cdot m^{-1}\cdot k^{-1}$ in the direction

parallel to the graphene plane, and that of the 10 vol% (7 wt%)graphene nanosheet/AlN composite reported by Yun et al. [8] is as low as 40 $W \cdot m^{-1} \cdot k^{-1}$. Similarly, carbon nanotubes have been reported to have a thermal conductivity up to 6600 $W \cdot m^{-1} \cdot k^{-1}$, whereas the AlN/CNT composite with 6 vol% (4 wt%) CNTs shows a relatively low λ of 62 $W \cdot m^{-1} \cdot k^{-1}$ [9]. All of these values are lower than the λ value of SG/AlN composite with 10 wt% SG prepared in this study at 76.82 $W \cdot m^{-1} \cdot k^{-1}$, indicating that SG had the least impact on the λ of AlN-based composites relative to other types of attenuating agents, which is credited to its spherical morphology

Table 1 Thermal properties of AlN-based composites with different second phases

Samples	Sintering method	Second phase content	Thermal diffusivity ($mm^2 \cdot s^{-1}$)	Thermal conductivity ($W \cdot m^{-1} \cdot K^{-1}$)	Refs.
Graphene Nanosheet/AlN	Hot-pressing	10 vol%		35.9 (Through-plane)	8
SWCNT /AlN	Hot-pressing	6 vol%		62	9
SiC/AlN	Plasma activated sintering	10 wt%	15	36	11
Graphene platelets/AlN	Spark plasma sintering	9.5 wt%	4.64	19.8	23
SiC/AlN	Hot-pressing	10 wt%		65	57
Graphene/AlN	Hot-pressing	10 wt%	18.95	39.7 (Through-plane)	58
Graphene platelets/AlN	Spark plasma sintering	8 wt%	19 37	43 (Through-plane) 84 (In-plane)	59
Spherical graphite/AlN	Hot-pressing	10 wt%	33.22	76.8 (Through-plane)	This work

As demonstrated in Figures 13(a) and (b), compared to the flake-shaped heterogeneous interface of AlN-based composites containing 2D flake graphite, ideally, the SG/AlN interface surrounding the SG also has be a spherical morphology, which

endows a remarkably lower cross-sectional area for the heterogeneous interface in the direction of thermal conduction. Additionally, in comparison with graphene, CNTs, and other 1D/2D nanoscale attenuating agents incorporated at the same volume fraction, microscale SG greatly reduces the number of heterogeneous interfaces in the AlN matrix. Zhang et al. [25] reported that the larger the particle size is, the lower the thermal conductive barrier it provides. It can be inferred that the slightly inhibited effect of the AlN grains due to the addition of SG extremely lessen the conductive barrier, this is in greatly contrast with the sharp decrease in the λ of graphene/AlN composites as the AlN particle size decreases [8,23,59]. All the above factors can considerably diminish the interfacial thermal resistance of the SG/AlN composites.

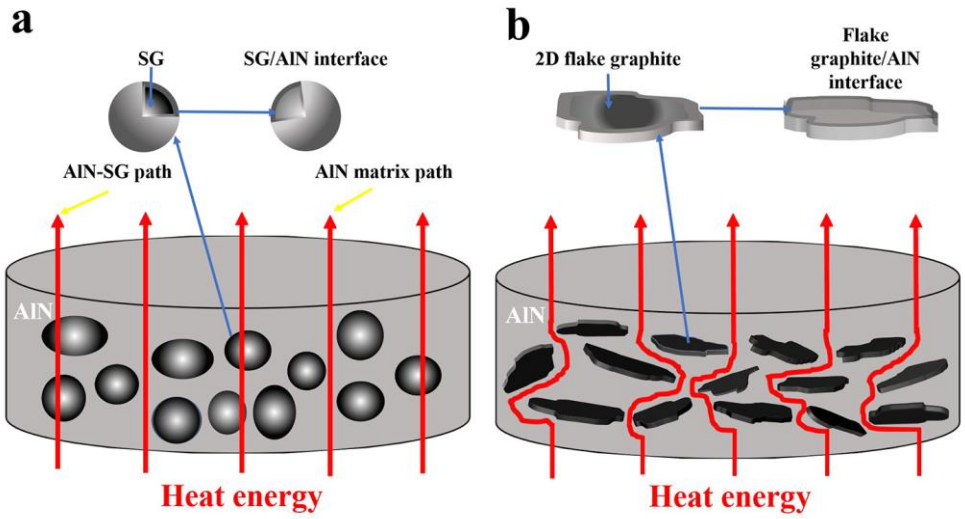

Fig. 13 The schematic diagram of thermally conductive path in composite filled with different shaped second phase, (a) spherical graphite, (b) 2D flake graphite

On the other side, since SG has a low-anisotropic λ, as distinguished from that of 2D materials with a uniaxially high λ, regardless of directions, there should be two thermally conductive paths within the SG/AlN composites. As indicated by the yellow

arrow in Figure 13(a), one is the SG-AlN thermally conductive path, and the other is the AlN matrix thermally conductive path, both of which hugely promotes the λ of the SG/AlN composites. The synergistic effect of the reduced interfacial thermal resistance and the low-anisotropic thermal conductivity of SG can deliver a higher λ for the SG/AlN composites. Moreover, the issue of the anisotropic λ for the composites containing 1/2D carbonaceous materials can also be alleviated by the weak orientation alignment of SG, further evidencing the potential of applying SG in the preparation of highly thermally conductive microwave attenuating materials with low anisotropy.

3.5 Dielectric Properties

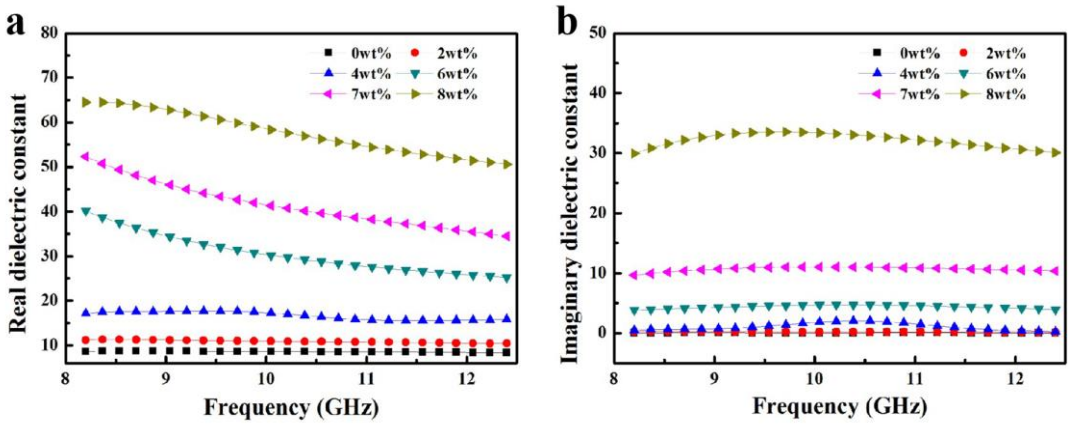

Fig. 14 Dielectric constant of SG/AlN composites with different SG contents

The microwave absorption performance of a non-magnetic absorption material is strongly dependent on its dielectric properties, such as the real dielectric constant ε', imaginary dielectric constant ε", and dielectric loss. The real and imaginary part of the dielectric constant refers to the polarization and lossy ability of the material under an applied electromagnetic field, respectively, and the dielectric loss is reflected by the loss tangent (tanδ=ε"/ε') [60]. The dielectric constant and dielectric loss as a function of microwave frequency (8.2 to 12.4 GHz) of the SG/AlN composites with different SG

contents are depicted in Figures 14 and 15, respectively. Both the dielectric constant and dielectric loss of the composites show a significant increment as the SG content increases from 0 wt% to 8 wt%. The ε', ε", and tan δ values of the monolithic AlN ceramic are 8.3 to 8.7, 0.03 to 0.07, and 0.004 to 0.008, respectively, showing an extremely low dielectric loss. While the ε', ε" and tan δ values for the 8 wt% composite are 50 to 64, 30 to 32 and 0.46 to 0.59, respectively, implying that the addition of SG has a pronounced improved effect on the dielectric loss of the SG/AlN composite materials.

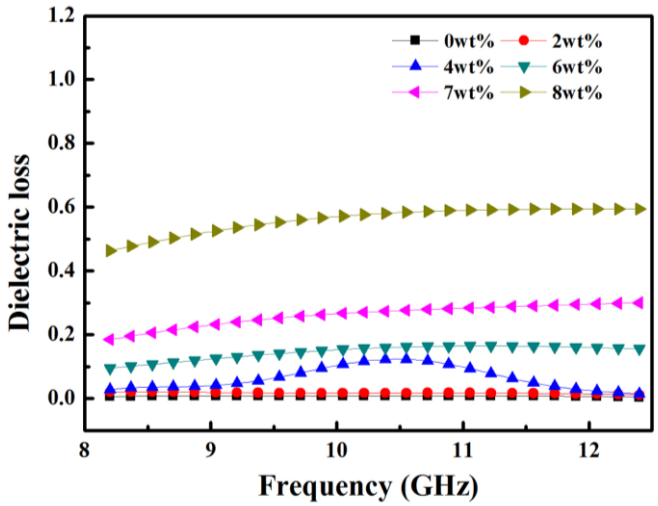

Fig. 15 Dielectric loss of SG/AlN composites with different SG contents

The real dielectric constant ε', which reflects the polarization ability of the material, is closely link with the ability of the material to store charges [61], and it is given by Equation (4) [60]:

$$\varepsilon' = \varepsilon_{\infty} + \frac{\varepsilon_s - \varepsilon_{\infty}}{1 + \omega^2 \tau^2} \tag{4}$$

where ε_s is the static dielectric constant, ε_{∞} is the optical dielectric constant, τ is the polarization relaxation time, and ω is the angular frequency. Inside the insulating AlN

matrix, the conductive phase, the SG particles, act as electrode plates and readily create a mini-capacitor effect. The shorter the distance between conductive SG particles, the further improved the capacitance of the composites, that is, the enhanced mini-capacitor effect. From this, the ability of the composites to store charges is sufficiently improved and in turn enhances the ε' value. The ε" value can be calculated using the following Equation [61]:

$$\varepsilon'' = \sigma / \omega \varepsilon_0 + \varepsilon_{relax} \quad (5)$$

where σ is the electrical conductivity of the material, ε_0 is the dielectric constant of free space (8.854×10^{-12} F·m^{-1}) [60], and ε_{relax} refers to the Debye relaxation loss. The imaginary part of the dielectric constant is proportional to the conductivity of the material, that is, conduction loss. As the conductive phase SG is incorporated into the matrix, it gradually forms a three-dimensional conductive network, which then significantly increases the electrical conductivity of the composite material and the electronic migration on the surface of the SG particles increase significantly, thereby enhancing the conduction loss of the material. It can be deduced from Equations (4) and (5) that the ε' and ε" values of the materials are closely related to the Debye relaxation loss. Based on the Debye theory, the Debye relaxation loss can be deduced from the by ε"–ε' curve, and the relationship between the real and imaginary parts of the dielectric constant can be described as follows [62]:

$$(\varepsilon'')^2 + (\varepsilon' - \frac{\varepsilon_s + \varepsilon_\infty}{2})^2 = (\frac{\varepsilon_s - \varepsilon_\infty}{2})^2 \quad (6)$$

If there is a polarization relaxation behavior existing in the material, a semicircle occurs in the ε"–ε' curve, which is called the Cole-Cole semicircle [62]. The ε" dependent ε'

curves of the SG/AlN composites with varying SG contents are displayed in Figure 16. No obvious semicircle is observed in the curves of the 0 wt% and 2 wt% SG samples, while the samples containing 4, 6, 7 and 8 wt% SG exhibit an identifiable Cole-Cole semicircle. This indicates that the SG addition leads to an obvious polarization relaxation behavior in the composite. Owing to the large mismatch between the electrical conductivity of AlN and SG in the SG/AlN composites, the interfacial charge polarization was strongly built as a result of the charge accumulation at the SG/AlN heterogeneous interfaces. Furthermore, the addition of the conductive phase SG not only increases the number of electrons in the composite material and enhances the electronic polarization, but also increases the number of pores and crystal defects produced during the sintering process, which form a large number of dipole polarization centers, resulting in dipole polarization. The multiple polarization processes resulting from the addition of SG significantly contribute to the enhancement of the ε' and ε" values. Aside from the typical Cole-Cole semicircle, a smooth tail is also observed in the ε"−ε' curves for the samples with 4 wt% and 8 wt% SG, which may be attributed to the excessive conduction loss in the composites [62]. Accordingly, in parallel with the variation of the real and imaginary dielectric constants, the loss tangent tan δ determined by ε' and ε" also exhibits an improvement, suggesting that the addition of SG enhances the dielectric loss capability of the composite.

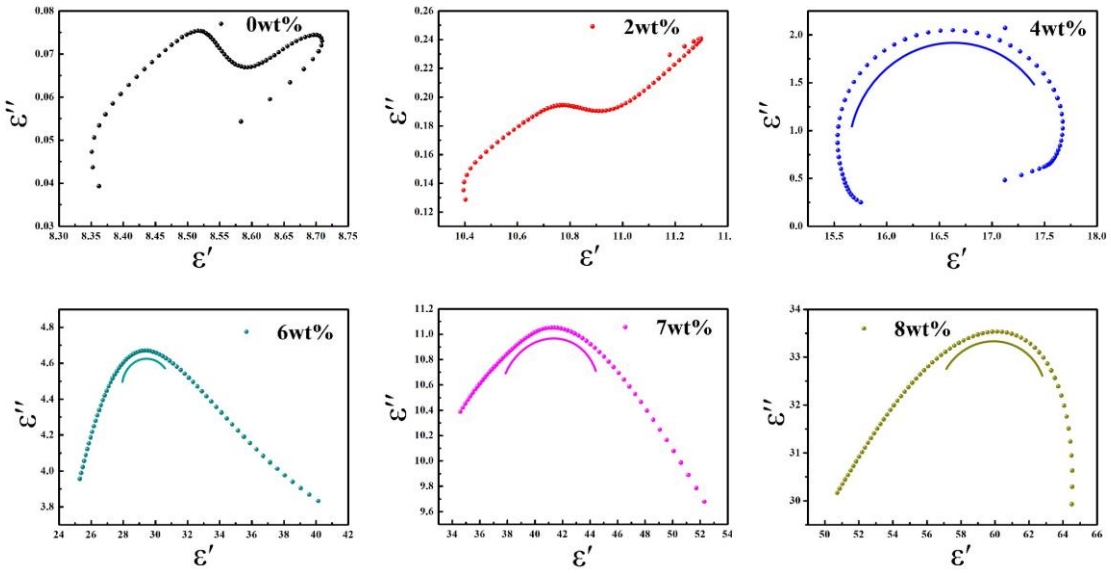

Fig. 16 The ε'-ε'' curves of SG/AlN composites with different SG contents

3.6 Microwave Absorption Properties

The microwave absorption property of material is usually characterized by the reflection loss (RL), which is expressed according to Equation (7) [63]:

$$RL = 20\lg\left|\frac{Z_{in} - Z_0}{Z_{in} + Z_0}\right| \tag{7}$$

where Z_0 is the impedance in free space, and Z_{in} is the incident impedance of the material surface, which can be obtained from Equation (8):

$$Z_{in} = Z_0\sqrt{\frac{\mu_r}{\varepsilon_r}}\tanh\left[j\frac{2\pi}{c}\sqrt{\mu_r\varepsilon_r}fd\right] \tag{8}$$

where f refers to the frequency of the electromagnetic wave, c is the speed of light (3×10^8 m/s), d denotes the material thickness, and ε_r and μ_r are the complex permittivity and complex permeability of the material, respectively (for non-magnetic materials, μ_r is commonly set to 1) [64]. RL is generally a negative value, and the smaller the value is, the stronger the absorption ability of the material. For instance, RL values below -4 dB

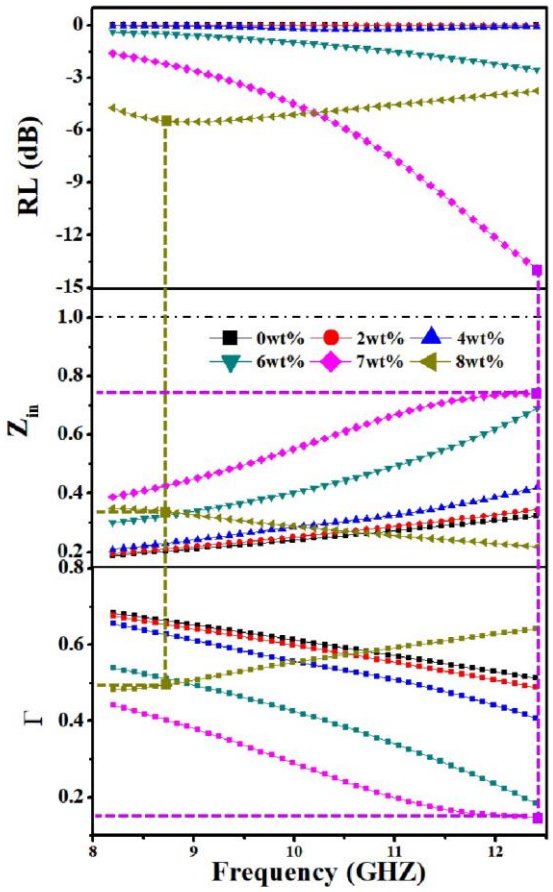

Fig.17 Reflection loss, incident impedance and reflection coefficient of SG/AlN composites with different SG contents

and -10 dB means that the material can absorb 36 % and 90 % of electromagnetic wave, respectively, and the latter case is considered as an effective absorption [63]. Figure 17 shows the RL of the SG/AlN composites as a function of SG contents at the thickness of 1 mm. In the X-band, as the SG content increases from 0 wt% to 8 wt%, the RL_{min} of the composites gradually decreases first, and then increases. When the SG content is less than 6 wt%, all the RL_{min} values are higher than -4 dB, indicating a poor absorption capability for electromagnetic waves. The RL value of 7 wt% sample significantly decreases with the increasing frequency in the X-band, and it shows the best absorption

performance with a RL_{min} value of -14 dB at 12.4 GHz. The improved absorption ability of the sample can be attributed to the enhanced dielectric loss, which is mainly derived from the interfacial polarization loss and conduction loss as a result of the addition of SG. Additionally, the improved charge storage ability resulting from the enhanced mini-capacitor effect also boosts the microwave absorption of the materials. Further increasing the SG content to 8 wt% deteriorates the microwave absorption ability of the composite, with a RL_{min} value of -5.5 dB.

Despite the RL_{min} and best effective absorbing bandwidth (EAB, ≦-10 dB) of -13.9 dB and 0.87 GHz, respectively, occurring for the 7 wt% SG sample, its overall absorption performance is not as satisfactory as enough. This is attributed to the impedance mismatch caused by the high dielectric constant of the composites. Excellent absorption materials should have, apart from a great loss ability for electromagnetic waves, a good impedance matching characteristic to reduce the reflection of electromagnetic waves on the surface of the material [62]. The ability of a material to reflect electromagnetic waves and the impedance matching characteristic of a material can be expressed by reflection coefficient Γ [65]:

$$\Gamma=|(Z_{in}-Z_0)/(Z_{in}+Z_0)| \quad (9)$$

A low Γ value supports a good impedance matching, that is, more electromagnetic waves could enter the material. The free-space impedance Z_0 value is fixed at 1, thus, it can be speculated from Equation (9) that a low Γ value, i.e., a well-matched impedance, can be obtained when the Z_{in} value is close to 1 [66]. To obtain a deeper understanding of the absorption ability of the SG/AlN composites, the calculated Z_{in} and Γ values as a

function of SG content are illustrated in Figure 17. It can be seen from the *RL*, Z_{in}, and Γ curves of the 7 wt% and 8 wt% samples that at the frequency with the maximum Z_{in} value (closest to 1), the materials exhibit the smallest Γ value. This indicates the RL_{min} value can be achieved at the best impedance matching, i.e., when there is the least reflection of electromagnetic waves. Overall, the Z_{in} values of all the SG/AlN composites are within in the range of 0 to 1 in the X-band, and they increase first and then decrease as the SG content increases from 0 wt% to 8 wt%, reaching the maximum at 7 wt% SG. Conversely, the reflection coefficient Γ of the composites gradually decreases as more SG is incorporated, attaining the minimum at 7 wt% SG (0.14 to 0.44), indicating the best impedance matching in the composite with 7 wt% SG, which is in good agreement with its absorption ability. The above results indicate that a good impedance is critical to the achievement of an excellent absorption property, which is highly dependent on the SG content. However, despite a high dielectric loss ability at a high SG content (8 wt%), the sample exhibits a weak absorption capability as a result of its poor impedance matching. On the whole, the AlN-based microwave attenuating composite ceramics, with its combined high thermal conductivity, improved dielectric loss, enhanced absorption ability and low anisotropy, are developed by employing SG as attenuating agent.

4 Conclusion

In this work, SG/AlN microwave attenuating composite ceramics with 0 to 16 wt% spherical graphite (SG) as the attenuating agent were prepared via hot-pressing sintering. The SG particles are homogeneously dispersed in the sintered bodies, displaying a

three-dimensional morphology and a negligible orientation alignment. The addition of SG impedes the sintering of the composites, while slightly influences on the growth of AlN grains. As the amount of SG added increases, the strength of the composites decreases monotonously, while the toughness initially increases and then decreases, with the maximum at 3.8 $MPa \cdot m^{1/2}$ for the composite with 4 wt% SG, demonstrating a moderate toughening effect. Despite the significant decrease in the thermal conductivity with SG addition, the SG/AlN composites exhibit a relatively higher thermal conductivity compared to other composites with non-spherical attenuating agents. The enhanced polarization loss, conduction loss, and mini-capacitor effect with the addition of SG (0 wt% to 8 wt%) significantly improve the dielectric constant and loss (0.004–0.008 to 0.46–0.59) of the composites within the frequency range of 8.2 GHz to 12.4 GHz. The absorption ability is enhanced as SG is added, with composite with 7 wt% SG having the best absorption performance with an RL_{min} of -14 dB at 12.4 GHz) and a wide EAB (0.87 GHz) at 7 wt% composite. In summary, the as-prepared SG/AlN composites are promising low anisotropic and highly thermally conductive attenuating materials.

Acknowledgement

This work was supported by the Priority Academic Program Development of Jiangsu Higher Education Institutions (PAPD), the Postgraduate Research&Practice Innovation Pro-gram of Jiangsu Province (KYCX20_0990), Qing Lan Project, the Program for Changjiang Scholars, Innovative Research Team in University (PCSIRT), IRT1146 and IRT15R35, and the Top-notch Academic Programs Project of Jiangsu

Higher Education Institutions (TAPP, PPZY2015B128).

References

[1] Zang XR, Lu YP. Preparation and dielectric properties at high frequency of AlN-based composited ceramic. *J Mater Sci: Mater Electron* 2020, **31**: 2826–2832.

[2] Chen CF, Perisse ME, Ramirez AF, et al. Effect of grain boundary phase on the thermal conductivity of aluminium nitride ceramics. *J Mater Sci* 1994, **29**: 1595–1600.

[3] Mikijelj B, Abe DK, Hutcheon R. AlN-based lossy ceramics for high average power microwave devices: performance-property correlation. *J Eur Ceram Soc* 2003, **23**: 2705–2709.

[4] Calame JP, Abe DK, Levush B, et al. Variable temperature measurements of the complex dielectric permittivity of lossy AlN-SiC composites from 26.5–40 GHz. *J Appl Phys* 2001, **89**: 5618.

[5] Chen YM, Pang L, Li Y, et al. Ultra-thin and highly flexible cellulose nanofiber/silver nanowire conductive paper for effective electromagnetic interference shielding. *Composites, Part A* 2020, **135**: 105960.

[6] Green M, Chen XB. Recent progress of nanomaterials for microwave absorption. *J Electroceramics* 2019, **5**: 503–541.

[7] Simsek ING, Andrés N, Eugenio G, et al. The effect of graphene nanoplatelets on the thermal and electrical properties of aluminum nitride ceramics. *J Eur Ceram Soc* 2017, **37**: 3721–3729.

[8] Yun C, Feng YB, Qiu T, et al. Mechanical, electrical, and thermal properties of graphene nanosheet/aluminum nitride composites. *Ceram Int* 2015, **41**: 8643–8649.

[9] Chakravarty A, Singh R, Roy S, et al. Aluminum nitride-single walled carbon nanotube nanocomposite with superior electrical and thermal conductivities. *J Am Ceram Soc* 2017, **100**: 3360–3364.

[10] Gu JL, Sang LL, Pan B, et al. Thermal conductivity and high-frequency dielectric properties of pressureless sintered SiC-AlN multiphase ceramics. *Mater* 2018, **11**:

969.

[11] Li PW, Wang CB, Liu HX, et al. Structural, thermal and dielectric properties of AlN–SiC composites fabricated by plasma activated sintering. *Adv Appl Ceram* 2019, **118**: 313–320.

[12] Chakravarty A, Singh R, Roy S, et al. Enhanced microwave absorption performance of double-layer absorbers Containing $BaFe_{12}O_{19}$ Ferrite and graphite nanosheet composites. *J Electron Mater* 2017, **100**: 3360–3364.

[13] Meng R, Zhang T, Yu HJ, et al. A facile coprecipitation method to Fe_xO_y/Fe decorated graphite sheets with enhanced microwave absorption properties. *Nanotechnol* 2019, 185704

[14] Qiu J, Qiu T. Fabrication and microwave absorption properties of magnetite nanoparticle-carbon nanotube-hollow carbon fiber composites. *Carbon* 2015, **81**: 20–28.

[15] Gupta KK, Abbas SM, Abhyankar AC. Carbon black/polyurethane nanocomposite-coated fabric for microwave attenuation in X & Ku-band (8-18GHz) frequency range. *J Ind Text* 2016, **46**: 510–529.

[16] Kim JB, Lee SK, Kim CG. Comparison study on the effect of carbon nano materials for single-layer microwave absorbers in X-band. *Compos Sci Technol* 2008, **68**: 2909–2916.

[17] Meng FB, Wang HG, Huang F, et al. Graphene-based microwave absorbing composites: A review and prospective. *Composites, Part B* 2018, **137**: 260–277.

[18] Liao XJ, Ye W, Chen LL, et al. Flexible hdC-G reinforced polyimide composites with high dielectric permittivity. *Composites, Part A* 2017, **101**: 50–58.

[19] Xu WH, Ding YC, Yu Y, et al. Highly foldable PANi@CNTs/PU dielectric composites toward thin-film capacitor application. *Mater Lett* 2017, **192**: 25–28.

[20] Liang HL, Wang CP, Huo YL, et al. AlN/CNT composites ceramics by spark plasma sintering. *Key Eng Mater* 2014, **603**: 570–573.

[21] Shen Y, Zhang H, Yang AM, et al. Outgassing property of carbon nanotube cathode with intense pulsed emission. *Acta Phys Sin* 2012, **61**: 103–109.

[22] Shen Y, Zhang H, Liu XG, et al. Outgassing mass spectrum analysis with intense

pulsed emission of carbon nanotube cathode. *Acta Phys Sin* 2011, **60**: 080702.

[23] Yin R, Zhang YB, Zhao W, et al. Graphene platelets/aluminium nitride metacomposites with double percolation property of thermal and electrical conductivity. *J Eur Ceram Soc* 2018, **38**: 4701–4706.

[24] Chen JK, Wang LM, Gui XC, et al. Strong anisotropy in thermoelectric properties of CNT/PANI composites. *Carbon* 2017, **114**: 1–7.

[25] Zhang XY, Shi ZQ, Zhang X, et al. Three dimensional AlN skeleton-reinforced highly oriented graphite flake composites with excellent mechanical and thermophysical properties. *Carbon* 2018, **131**: 94–101.

[26] Fan YZ, Yang HB, Li MH, et al. Evaluation of the microwave absorption property of flake graphite. *Mater Chem Phys 2009*, **115**: 696–698.

[27] Yuan GM, Li XK, Dong ZJ, et al. Graphite blocks with preferred orientation and high thermal conductivity. *Carbon* 2012, **50**: 175–182.

[28] Zheng WE, Wong SC. Electrical conductivity and dielectric properties of PMMA/expanded graphite composites. *Compos Sci Technol* 2003, **63**: 225–235.

[29] He F, Lau S, Chan HL, et al. High dielectric permittivity and low percolation threshold in nanocomposites based on poly (vinylidene fluoride) and exfoliated graphite nanoplates. *Adv Mater* 2009, **21**: 710–715.

[30] Wang P, Cheng LF, Zhang Y, et al. Electrospinning of graphite/SiC hybrid nanowires with tunable dielectric and microwave absorption characteristics. *Composites, Part A* 2018, **104**: 68–80.

[31] Du YC, Liu T, Yu B, et al. The electromagnetic properties and microwave absorption of mesoporous carbon. *Mater Chem Phys* 2012, **135**: 884–891.

[32] Torğut G, Biryan F, Demirelli K. Effect of graphite particle fillers on dielectric and conductivity properties of poly (NIPAM-co-HEMA). *Bull Mater Sci* 2019, **42**: 244.

[33] Sun MY, Bai YH, Li MX, et al. Improved toughness and electromagnetic shielding-effectiveness for graphite-doped SiC ceramics with a net-like structure. *J Eur Ceram Soc* 2018, **38**: 5271–5281.

[34] Zhang Y, He PG, Yuan JK, et al. Effects of graphite on the mechanical and microwave absorption properties of geopolymer based composites. *Ceram Int* 2017,

43: 2325–2332.

[35] Sevostianov I, Cross property connection between the electric and the thermal conductivities of copper graphite composites. *Mech Mater 2012,* **45**: 20–33.

[36] Marinopoulo AG, Reining L, Olevano V, et al. Anisotropy and interplane interactions in the dielectric response of graphite. *Phys Rev Lett* 2002, **89**: 076402.

[37] Zeng FK, Xue C, Ma HB, et al. High thermal conductivity and anisotropy values of aligned graphite flakes/copper foil composites. *Mater* 2020, **13**: 46.

[38] Li WJ, Liu Y, Wu GH. Preparation of graphite flakes/Al with preferred orientation and high thermal conductivity by squeeze casting. *Carbon* 2015, **95**: 545–551.

[39] Yoshio M, Wang H, Fukuda K. Spherical carbon-coated natural graphite as a lithium-ion battery-anode material. *Angew Chem, Int Ed* 2003, **42**: 4203–4206.

[40] Wu YS, Wang YH, Lee YH. Performance enhancement of spherical natural graphite by phenol resin in lithium ion batteries. *J Alloys Compd* 2006, **426**: 0–222.

[41] Li M, Fang ZR, Wang SK, et al. Thermal conductivity enhancement and heat transport mechanism of carbon fiber z-pin graphite composite structures. *Compos* 2019, **172**: 603–611.

[42] Huang D, Tian ZB, Cui W, et al. Effects of Y_2O_3 and yttrium aluminates as sintering additives on the thermal conductivity of AlN ceramic substrates. *Ceram Int* 2018, **44**: 20556–20559.

[43] Nakano H, Watari K, Hayashi H, et al. Microstructural characterization of high-thermal-conductivity aluminum nitride ceramic. *J Am Ceram Soc* 2002, **85**: 3093–3095.

[44] Narang V, Korakakis D, Seehra MS. Electronic state of Er in sputtered AlN:Er films determined by magnetic measurements. *J Appl Phys* 2014, **116**: 213911.

[45] Jiang SH, Cheong JY, Nam JS, et al. High-density fibrous polyimide sponges with superior mechanical and thermal properties. *ACS Appl Mater Interfaces* 2020, **12**: 19006–19014.

[46] Wang F, Chen L, Li HL, et al. N-doped honeycomb-like porous carbon towards high-performance supercapacitor. *Chin Chem Lett* 2020, **56**: 3935–3938.

[47] Yan DF, Guo L, Xie C, et al. N, P-dual doped carbon with trace Co and rich edge

sites as highly efficient electrocatalyst for oxygen reduction reaction. *Sci China Mater* 2018, **61**: 679–685.

[48] Zhao CL, Wu YX, Liang HL, et al. N-doped graphene and TiO_2 supported manganese and cerium oxides on low-temperature selective catalytic reduction of NO_x with NH_3. *J Adv Ceram* 2018, **7**: 197–206.

[49] Zhou SZ, Zhou GY, Jiang SH, et al. Flexible and refractory tantalum carbide-carbon electrospun nanofibers with high modulus and electric conductivity. *Mater Lett 2017*, **200**: 97–100.

[50] Kuang B, Song WL, Ning MQ, et al. Chemical reduction dependent dielectric properties and dielectric lossmechanism of reduced graphene oxide. *Carbon* 2018, **127**: 209–217.

[51] Yu JJ, Liu SW, Duan GG, et al. Dense and thin coating of gel polymer electrolyte on sulfur cathode toward high performance Li-sulfur battery. *Compos Commun* 2020, **19**: 239–245.

[52] Duan GG, Liu SW, Jiang SH, et al. High-performance polyamide-imide films and electrospun aligned nanofibers from an amidecontaining diamine. *J Mater Sci* 2019, **54**: 6719–6727.

[53] Cho WS, Cho MW, Lee JH, et al. Effects of h-BN additive on the microstructure and mechanical properties of AlN-based machinable ceramics. *Mater Sci Eng A* 2006, **418**: 61–67.

[54] Chen C, Pan LM, Li XY, et al. Mechanical and thermal properties of graphene nanosheets/magnesia composites. *Ceram Int* 2017, **43**: 10377–10385.

[55] Wang XL, He XB, Zhang R, et al. Interface and properties of copper matrix composites reinforced with TiC coated spherical graphite. *Mater Res Express* 2019, **6**: 116307.

[56] Schlichting KW, Padture NP, Klemens PG. Thermal conductivity of dense and porous yttria-stabilized zirconia. *J Mater Sci 2001*, **36**: 3003–3010.

[57] Landon M, Thevenot F. Thermal conductivity of SiC-AlN materials. *J Eur Ceram Soc* 1991, 271–277.

[58] Rutkowski P, Kata D, Jankowski K, et al. Thermal properties of hot-pressed

aluminum nitride–graphene composites. *J Therm Anal Calorim* 2016, **124**: 93–100.

[59] Baskut S, Cinar A, Turan S, Directional properties and microstructures of spark plasma sintered aluminum nitride containing graphene platelets. *J Eur Ceram Soc* 2017, **37**: 3759–3772.

[60] Guo X, Feng YR, Lin X, et al. The dielectric and microwave absorption properties of polymer-derived SiCN ceramics. *J Eur Ceram Soc* 2018, **38**: 1327–1333.

[61] Zhou L, Cui S, Zhai Y, et al. Dielectric and microwave absorption properties of plasma sprayed Cr/Al_2O_3 composite coatings. *Ceram Int* 2015, **41**: 14908–14914.

[62] Qin M, Lan D, Wu GL, et al. Sodium citrate assisted hydrothermal synthesis of nickel cobaltate absorbers with tunable morphology and complex dielectric parameters toward efficient electromagnetic wave absorption. *Appl Surf Sci* 2020, **504**: 144480.

[63] Li XL, Yin XW, Song CQ, et al. Self-assembly core–shell graphene-bridged hollow MXenes spheres 3D foam with ultrahigh specific EM absorption performance. *Adv Funct Mater* 2018, **28**: 1803938.

[64] Liu JL, Liang HS, Wu HJ. Hierarchical flower-like Fe_3O_4/MoS_2 composites for selective broadband electromagnetic wave absorption performance. *Composites, Part A* 2020, **130**: 105760.

[65] Zhou W, Yin RM, Long L, et al. Enhanced high-temperature dielectric properties and microwave absorption of SiC nanofibers modified Si_3N_4 ceramics within the gigahertz range. *Ceram Int* 2018, **44**: 12301–12307.

[66] Lou ZC, Li R, Wang P, et al. Phenolic foam-derived magnetic carbon foams (MCFs) with tunable electromagnetic wave absorption behavior. *Chem Eng J 2020*, **391**: 123571.